Sustainable Macromolecules Assisted Preparation of Cross-linked, Ultralight, Flexible Graphene Aerogel Sensors toward Low-Frequency Strain/Pressure to High-Frequency Vibration Sensing

Zhihui Zeng,* Na Wu, Weidong Yang, Hao Xu, Yaozhong Liao, Mirko Luković, Shanyu Zhao, Zhongqing Su, and Xuehong Lu *

Prof. Z. Zeng

Key Laboratory for Liquid-Solid Structural Evolution and Processing of Materials, Ministry of Education and School of Materials Science and Engineering, Shandong University, Jinan, Shandong, 250061, China

*E-mail: zhihui.zeng@sdu.edu.cn (Z. Zeng),

Prof. Z. Zeng, Prof. X. Lu,

School of Materials Science and Engineering, Nanyang Technological University, 50 Nanyang Avenue, Singapore 639798, Singapore

*E-mail:asxhlu@ntu.edu.sg (X. Lu);

Dr. N. Wu

Department of Chemistry and Applied Biosciences, ETH Zurich, CH-8093 Zurich, Switzerland

Prof. W. Yang

School of Aerospace Engineering and Applied Mechanics, Tongji University, Shanghai 200092, China

Assoc. Prof. H. Xu

School of Aeronautics and Astronautics, Dalian University of Technology, Dalian, China

Dr. Y. Liao, Prof. Z. Su

Department of Mechanical Engineering, The Hong Kong Polytechnic University, Kowloon, Hong Kong

Dr. M. Luković, Dr. S. Zhao

Swiss Federal Laboratories for Materials Science and Technology (EMPA), Überlandstrasse 129, 8600 Dübendorf, Switzerland

Keywords: sensor, graphene aerogel, crosslink, sustainable, composites

Abstract: Ultralight and highly flexible aerogel sensors, composed of sustainable macromolecules derived carbon crosslinked reduced graphene oxide, are prepared via facile freezing-drying and thermal annealing. The synergistic combination of crosslinked graphene nanosheets and micrometer-sized honeycomb pores gives rise to the exceptional properties of the aerogels, including superior compressibility and resilience, good mechanical strength and durability, satisfactory fire-resistance, and outstanding electromechanical sensing performances. The corresponding aerogel sensors, operated at an ultralow voltage of 0.2 V and with power consumption below 2.0 mW, can efficiently respond to a wide-range strains (0.1 %-80 %) and pressures (13-2750 Pa) even at temperatures beyond 300 °C. Moreover, ultrahigh pressure sensitivity of 10 kPa^{-1}, and excellent sensing stability and durability are accomplished. Most importantly, the aerogel sensors sense the vibration signals with ultrahigh frequencies of up to 4000 Hz at more than 1, 000, 000 cycles, significantly outperforming those of other sensors. These enabled us to successfully demonstrate the exceptional performance of the crosslinked graphene based biomimetic aerogels for sensitive monitoring of mechanical signals, as wearable devices for monitoring human motions, and for non-destructive monitoring of cracks on engineering structures, showing the great potential of the aerogel sensors as next-generation electronics for a wide range of applications.

Introduction

Recently, three-dimensional (3D) porous carbon materials as low-density, compressible strain and/or pressure sensors that can sense mechanical deformations by measuring the change in electrical signals have shown great potentials in a wide of applications, such as aerospace, human-machine interfaces, human motion detection, and structural health monitoring (SHM).[1, 2-7] Graphene, with its single-layer carbon atoms arranged into a honeycomb-like two-dimensional (2D) nanostructure,[4-6, 8, 9] has received tremendous interest for constructing porous aerogel based strain/pressure sensors due to its good conductivity, easy assembly, high stability, and excellent mechanical strength and flexibility.[10, 11] These 3D graphene aerogel sensors prepared via various methods such as solvent thermal, freeze-casting, or chemical vapor deposition, exhibit low density, good mechanical elasticity, and a wide sensing strain/pressure range,[2, 12-16] outperforming the traditional sensors made of metal and semiconductors.[5, 17] However, inherently weak connections and fragile joints of the graphene networks result in an undesirable mechanical strength and flexibility as well as a poor fatigue resistance of the 3D aerogel sensors under low density ranges,[3, 16-18] which is not beneficial for the stability and durability in practical applications. Moreover, the graphene aerogel sensors are mainly focused on detecting the quasi-static or low-frequency dynamic strain/pressure, which might be attributed to the poor interactions of the graphene nanosheets leading to the difficulty in rapidly responding high-frequency mechanical signals. Sensing mechanical signals with higher frequencies such as acoustical or vibration signals of the lightweight graphene aerogels is highly desirable for many application scenarios yet remains rarely reported. [19-22]

Generally, in order to achieve the desired electrical, mechanical, and electromechanical sensing performances, a rational design of the building constituents and geometrical structures for the graphene-based 3D monoliths is crucial. Qiu *et al.* enhanced face-to-face interactions of graphene sheets in graphene aerogels via an ultrahigh-temperature annealing treatment, leading to largely improved mechanical strength and resilience of the resultant sensors at densities below 1.0 mg/cm^3.[18] The aerogels showed an unprecedented pressure sensitivity of up to 15 kPa^{-1} despite a maximum sensing pressure of merely 100 Pa. Inorganic one-dimensional carbon nanotubes (CNTs) were employed to prevent sliding between graphene sheets and enhance the stiffness of the cell walls in graphene-based aerogels, resulting in improved mechanical strength and resilience.[23, 24] Nevertheless, the construction processes of these graphene-based aerogel sensors usually required some special treatments such as unavoidable surface functionalization or treatment at extremely high temperatures to efficiently crosslink the graphene layers. Organic molecules were also employed to physically crosslink the graphene layers and enhance the interactions among the 2D layers, thereby improving the flexibility and elasticity of the resultant sensors. [9, 25, 26, 27] For instance, mechanically flexible and elastic reduced graphene oxide (RGO) embedded polyimide composite foams were prepared with high pressure sensitivity of up to 0.18 kPa^{-1} and excellent durable stability.[25] Nevertheless, the poor thermal resistance and limited mechanical strength or rigidity of such composite architectures, as well as the predominantly fossil-fuel-based origin of the employed polymers, have limited their practical applications as lightweight, robust, and temperature-tolerance sensors.[27] In general the introduction of polymers also significantly reduces the conductivity of the graphene-based porous architectures, resulting in a high operating voltage or high energy

consumption of the sensors. Therefore, designing precise constituents to efficiently enhance the interactions among graphene nanosheets in the cellular macrostructures for high-performance sensing applications remains highly desirable. Other than that, it has also been demonstrated that biomimetic aligned porous graphene aerogels could exhibit better mechanical strength and resilience than random cellular architectures, [7, 14, 15, 19, 28] showing the potential of manipulating pore microstructures for improving electromechanical sensing performance, especially for the high-frequency sensing capability. For instance, the aligned porous graphene-based aerogels were considered to be beneficial for sensing high-frequency vibration of 2000 Hz despite lacking the durability and application explorations.[20] In short, designing robust graphene-based aerogels that could simultaneously achieve ultralow density, excellent mechanical flexibility and sensing sensitivity, fast response, diverse sensing capabilities associated with efficient applications, remarkable durability, and low energy consumption via a straightforward, facile, and scalable approach remains urgently required yet a great challenge.

To address the aforementioned challenge, in this work, sustainable hydrophilic macromolecules, including but not limited to biomass lignin, [7, 29, 30] were utilized as both the crosslinkers and boosters for the assembly of graphene oxide (GO) layers into microhoneycomb porous monoliths via straightforward and facile ice-templated freeze-drying [31-33]. This enabled us to facilely prepare ultralight, flexible, and robust macromolecule derived carbon crosslinked graphene aerogels with biomimetic aligned pore morphology [7, 32, 34] via a scalable thermal annealing process. The sustainable macromolecule-derived carbons are instrumental in the excellent chemical and thermal stabilities and considerable conductivity. [6, 7, 29, 30, 35] Moreover, the carbons effectively crosslink the

graphene layers so as to improve the interactions among graphene layers, leading to good mechanical strength, excellent stability and durability, and significantly improved electromechanical sensing performances of the aerogel sensors. Our aerogel sensors are capable of efficiently detecting a wide-range of strains, between 0.1% and 80.0%, even at a temperature beyond 300 ℃ while operating at a low voltage level (0.2V) and low energy consumption rate (< 2.0 Mw). The aerogel sensors also show ultrahigh pressure-sensitivity of around 10 kPa^{-1} in a wide pressure range, from 13 to 2750 Pa, and excellent sensing stability and durability. Moreover, they can detect vibrations at an ultrahigh frequency of 4000 Hz with an extremely large number of cycles (＞1, 000, 000 cycles), significantly outperforming other reported carbon monoliths. Our ultralight and highly flexible sensors are compatible with the human body to detect pulse vibration and a variety of human motions including frequencies and amplitudes of wrist and finger bending. More intriguingly, the high-frequency vibration sensing capability is also efficiently employed for non-destructive monitoring of cracks on engineering structures. This thus demonstrates the promising application potentials of our ultralight, highly flexible, robust graphene-based biomimetic porous aerogels as next-generation electronics.

Results and Discussion

To fabricate the crosslinked graphene-based biomimetic aerogel sensors, the first step is to mix the aqueous solution of a selected type of macromolecules with a GO aqueous dispersion to facilitate their assembly into microhoneycomb structures via directional freeze-drying. In the unidirectional freezing process, [33, 34] a steep temperature gradient in the mixed aqueous dispersion is generated (**Figure 1**a), which leads to the rapid unidirectional growth of ice crystals (Figure 1b). Abundant

hydrophilic polar surface functional groups of both GO and the organic macromolecules are beneficial for the stability of the mixed dispersion (Figure S1a-f). The macromolecules employed in this work include lignin, polyvinyl alcohol (PVA) and polydopamine (PDA)[30], respectively. The GO layers which can be well attached with organic macromolecules due to the hydrogen interactions are excluded from the surface of ice crystals, producing a microhoneycomb GO-based hybrid aerogel after the sublimation of ice crystals in the freeze-drying process (Figure S1g). Then, by annealing, the RGO/macromolecule-derived carbon hybrid aerogels are obtained. The flexible organic macromolecules, has relatively high diffusibility and hence could boost the migration of GO in the freezing process, while it could also effectively bind the GO layers in the GO based hybrid aerogels, ultimately resulting in the intercalation of macromolecule-derived carbon between RGO layers and the effective crosslink of graphene layers by the carbons in the graphene/carbon hybrid aerogels (Figure 1b, Figure S2a). Herein lignin and the corresponding lignin-derived carbon (LDC) will be used as the representative to demonstrate the effectiveness of our approach and illustrate the underlying mechanisms. This led to the efficient construction of the ultralight (~3.5 mg/cm^3) yet robust, highly flexible crosslinked graphene aerogels (Figure 1c), which exhibit biomimetic microhoneycomb structure with unidirectional penetrating pores (Figure 1d, e).

XRD patterns and Raman spectra reveal the properties and structure of the crosslinked graphene aerogel sensors. In the XRD patterns (Figure S2b), a sharp diffraction peak near 26.0° caused by the graphite structure and a broad peak around 24.5° due to carbon show the successful preparation of the RGO and LDC aerogels, respectively. The sharp peak around 22.5° of the hybrid ROG/LDC aerogels corresponds to an increased interlayer spacing of graphene, resulting from the incorporation

of LDC between the stacked graphene layers. Typical 2D peaks in Raman spectra (Figure S2c) of the hybrid aerogels further confirm the existence of graphene in the aerogels, while this peak is absent in the Raman spectrum of LDC. The ratio of D-band intensity (I_D, the sp^3 carbon atoms in amorphous carbon and defects at 1340-1350 cm^{-1}) to G-band intensity (I_G, the stretching of sp^2 carbon atoms in graphitic 2D hexagonal lattice at 1580-1590 cm^{-1}) increases significantly from 0.86 to 1.28 when the GO is reduced to RGO, which is ascribed to the decreased average size of the sp^2 domain after thermal annealing treatment of GO.[2, 29, 36] The I_D/I_G value of the aerogels decreases regularly with increasing LDC content, further indicating the efficient penetration[43] of LDC into the graphene layers in the aerogels. Thus, the hybrid aerogels have ultrathin cell walls of ~10 nm with good integrity due to the efficient crosslink of the graphene layers (Figure 1f, Figure S3). By contrast, the cell walls of the RGO aerogel consist of smaller pieces of holey graphene layers that are much less interconnected (Figure S3c) due to the poor interlayer interactions among graphene nanosheets. The crosslinked, robust graphene-based cell walls with the help of the LDC are thus instrumental in enhancing the mechanical strength and stability of the aerogels. The shape of the crosslinked graphene-based aerogels is maintained when burnt under an ethanol flame (Figure S4, Video S1 in supporting information), further demonstrating their good mechanical stability and excellent fire-resistance. In addition, like with other honeycomb-like carbon aerogels, [7, 14, 24] compression deformations of our microhoneycomb aerogels upon compression in the direction normal to the pore channels are also reversible. The crosslinked graphene microhoneycomb aerogels show excellent reversibility under various compressive strains ranging from 10 % to 80 % (Figure 1g). Finite element (FE) simulation is efficiently employed to prove an extremely tiny true strain of the ultrathin

cell walls for the micro honeycomb-like porous graphene-based monoliths upon a large deformation of 80% (Figure 1h, Figure S5). In contrast, at a large strain of more than 70%, the neat microhoneycomb-like LDC aerogels cannot recover completely (Figure S6), proving the significance of a rational design of both the constituents and pore structure. In addition, the dynamic mechanical performances of the crosslinked graphene aerogels under various frequencies are revealed to support the potential sensing ability in a high-frequency range (Figure 1i). The storage modulus increases while the loss modulus (and tan delta, the ratio of energy dissipated to energy stored in the deformation cycle) decreases considerably with increasing frequency, showing that the aerogel can maintain the elasticity with insignificant viscosity even under high-frequency conditions. Since the storage and loss moduli of the aerogels are also almost constant in a wide-range of temperatures, from room temperature to over 300 °C, the crosslinked graphene aerogels show excellent temperature-independent mechanical performance, which is beneficial for the application in a harsh environment (Figures 1j). In short, the aforementioned favorable structural features and properties make our ultralight, robust, crosslinked graphene-based aerogels a class of promising materials for stable, high-performance electromechanical sensors.

The compressions of the crosslinked graphene biomimetic aerogels cause an increase in current when a fixed voltage of 0.2 V is applied (**Figure 2**a-e). The aerogels show a reversible and repeatable current change ratio ($\Delta I/I_0 = (I-I_0)/I_0$, where I_0 and I are the current values in the initial and compression state, respectively) [27, 31, 37] at cyclic compressive strains from 10% to 70 % (Figure 2a). A higher compressive strain corresponds to a larger $\Delta I/I_0$ value. At the same compressive strain of 50%, $\Delta I/I_0$ corresponds to the aerogel sensors' strain sensitivity, which increases with increasing

LDC content (Figure 2b). The $\Delta I/I_0$ value can be as large as 28.0 for aerogels with 79.2 wt% LDC, which is much higher than that of neat RGO aerogels (~3.0). This can be ascribed to the fact that the interactions and crosslinking between graphene layers are improved by incorporating more LDC, which leads to more aligned cell walls with better integrity (Figure S3). As a result, more efficient contacts between adjacent conducting cell walls are formed when the same compressive strain is applied. This contributes to a more significant change in the electrical signals. Moreover, more LDC between graphene layers reduces the initial contacts between the RGO layers and thus decreases initial conductivity of the hybrid aerogels, leading to a larger change of conductivity upon the compressive deformation. PDA- or PVA-derived carbons (PDAC (C-2) or PVAC (C-3)) in the corresponding graphene/carbon hybrid aerogels also give rise to the similar sensing behavior (Figure 2c, d). For example, the graphene/C-2 hybrid aerogels can increase the $\Delta I/I_0$ value to ~40. This clearly demonstrates the critical role played by the more macromolecule derived carbons (LDC, PVAC and PDAC) in improving sensing performances of the graphene-based aerogels. Certainly, the graphene layers significantly enhance the mechanical stability and durability when cycling under large deformation strains. Therefore, although LDC aerogels show relatively high $\Delta I/I_0$ values of around 30 in the initial tens of compression cycles, a better balance between elasticity and sensitivity is attainable with the carbon crosslinked graphene biomimetic aerogels.

Aerogels with a higher density of 5.5 mg/cm^3 are also prepared by simply increasing the concentration of the GO/lignin dispersion. At compressive strains above 30%, a higher strain sensitivity is displayed, in contrast to that of aerogels with a lower density of 3.5 mg/cm^3 (Figure 2f). This can be attributed to more intact cell walls that derive from more building blocks, and the

formation of more contacts between adjacent cell walls of the higher density aerogels. However, at strains below 30%, higher density aerogels show a lower strain sensitivity. This can be attributed to the presence of more building blocks per volume in the aerogel and therefore an initial presence of more conductive paths. As a result, there is less change in the electrical signals upon low strains and the bending of the cell walls becomes the dominant factor responsible for the increase in conductivity. In short, the strain sensing properties of the hybrid aerogels are determined by both the structure and amount of the building blocks in the aerogels.

Moreover, it is worthy noted that the high sensing performance allows the crosslinked graphene-based aerogels to detect subtle deformations that are as small as 0.1 % (Figure 2g, h). Under the cyclic compressive deformations between 5.0 % to 0.1 %, the current change is displayed with good stability and repeatability (Figure S7). Therefore, the aerogel sensors could act as high-performance compressive strain sensors with outstanding strain sensitivity, wide-range sensing strain, considerable mechanical durability, and excellent high-temperature stability. The stable macromolecule derived carbon crosslinked graphene aerogels also show remarkable and stable electromechanical sensing performance even at a high temperature of 300 ℃, showing the high potentials for sensing applications in a harsh environment (Figure 2i).

The excellent mechanical properties and resilience of the crosslinked graphene aerogels could endow the aerogels with high pressure sensing performances including wide sensing pressure range, high sensitivity, and excellent durability. The pressure sensitivity (*S*) is quantitatively defined as the ratio of $\Delta I/I_0$ to the applied pressure/stress.[7, 11, 18, 38] In the cyclic testing process, a gradual increase in the pressure from 0.75 to 2.75 kPa induces the corresponding change in $\Delta I/I_0$ with excellent

reversibility and repeatability **(Figure 3**a-b). Furthermore, a good liner relationship between the $\Delta I/I_0$ and applied pressure is observed in a wide pressure range (0-2.75 kPa). The *S* in the linear region is calculated to be around 10 kPa^{-1}, which is comparable to the maximum values of the present piezoresistive sensors reported in the literature (Figure 3c, Table S1). Such aerogel sensors with both a wide linear sensing pressure range and excellent sensitivity are very useful for quantitatively monitoring mechanical deformations.

The capability to detect subtle and rapid pressure changes is also important for many pressure sensing applications. By gradually decreasing the applied cyclic pressure from 683 to 13 Pa, the current of the aerogels changes accordingly with good reversibility and repeatability (Figure 3d, e). Moreover, under cyclic loadings, the $\Delta I/I_0$ change shows good repeatability and reversibility for more than 1000 cycles, highlighting the excellent sensing durability and reliability of our aerogel pressure sensors (Figure 3f).

In contrast to the polymer-based sensors with intrinsic viscoelastic characteristics[18], electrical signals of the carbon aerogels can change instantly and then remain constant upon rapidly loading/unloading pressure. To demonstrate the excellent performance of our sensors in this aspect, pressure sensing performances at various compressive speeds have been tested, *e.g.*, a pressure (350-600 Pa) with frequencies varying from 0.005 to 0.4 Hz is applied (**Figure 4**a) while a similar $\Delta I/I_0$ value is observed. As we have known that the carbon crosslinked graphene-based aerogel can maintain the elasticity with insignificant viscosity even under high-frequency conditions. Therefore, a sensing performance test under high-frequency mechanical vibrations has been designed to further investigate the aerogels' responses to broadband sensing frequency. Briefly, a vibration shaker is

used to excite a solid beam to which a piece of aerogel has been attached, causing the loading-unloading of pressure on the sensor at high frequencies (Figure 4b). The aerogel sensors showcase a stable, reversible and repeatable electrical response to vibrations from 400 to 4000 Hz, as displayed in Figure 4c-e. In such as high frequency of 4000 Hz, a response time of merely 0.125 ms is achieved, further demonstrating the advancement of the crosslinked graphene aerogels in detecting high-frequency mechanical signals in practical applications. To the best of our knowledge, the sensing frequency of our crosslinked, ultralight graphene aerogel is much higher than that of other typical strain/pressure sensors ever reported (Table 1). Larger amplitude of the vibration signals further contributes to the higher deformation of the aerogel sensors and thus the output voltage signals, showing the quantified sensing capability to high-frequency signals. More importantly, the crosslinked, stable graphene aerogel sensors can detect the ultrahigh-frequency vibrations with an extremely large number of cycles ($>1,000,000$ cycles), significantly outperforming those of other reported sensors. In summary, the crosslinked graphene-based biomimetic aerogel sensors exhibit excellent high-frequency pressure sensing performances, demonstrating their potential as broadband sensors for monitoring mechanical signals.

The excellent electromechanical sensing performances of the robust, crosslinked graphene-based biomimetic aerogels are promising for practical applications. Touching or pressing the aerogel sensors can be detected efficiently by observing the corresponding current signals (**Figure 5**a, Video 2 in supporting information). The current inside the aerogel increases immediately in response to the pressure induced by a touch of the finger. The current can also recover quickly when the pressure is released. Although the touch speed is high, the sensor detects and distinguishes each touch clearly,

which is consistent with its ability to respond to pressures at various frequencies. Owing to their great mechanical robustness and flexibility, the aerogel sensors can easily be attached to the human body as a wearable device for detecting human motions. Current signals of aerogel sensors attached to the wrist show that the subtle beat of the pulse and the bending movement of the wrist/finger are well detected (Figure 5b, c, d). The slow and fast movements of the wrist are also distinguished well. When the sensor is attached to a finger that bends slightly and then keeps steady, the current of the aerogel sensor initially increases due to the introduced pressure caused by the bending and then keeps stable. A larger bending radius of the finger leads to a higher compressive strain/pressure applied on the sensors, and thus a higher change in current. Leveraging on the high sensitivity to high-frequency structural vibrations, the aerogel sensors are employed for damage detection in engineering structure, which is of critical importance for the application of SHM. As a representative example shown in Figure 5e, the distribution of the frequency response functions (FRFs) of a cantilever beam are measured accurately using an aerogel sensor, indicating the capacity of the sensor in measuring structural strains not only in time domain, but also in frequency domain. Such capacity enables the sensor to capture the subtle decrease in eigen-frequencies, as can be recognized from the shift of FRFs, which can be utilized for the identification of a generated crack in the beam.[22] In short, on the basis of the great performances demonstrated above, the ultralight, crosslinked graphene-based biomimetic aerogels are useful as novel wearable sensors for detecting various human movements, and for non-destructive monitoring of cracks on engineering structures.

Conclusions

In this study, a type of ultralight, highly flexible, crosslinked graphene-based biomimetic aerogels have been successfully fabricated from GO and sustainable hydrophilic macromolecules, such as biomass lignin, via facile directional freeze-drying and thermal annealing. The structural and morphological studies show that macromolecule-derived carbons inserted between graphene nanolayers can enhance the interactions of graphene in the cell walls of the aerogels, leading to more cell walls with better integrity, and hence remarkable mechanical strength and flexibility, and excellent mechanical resilience and durability under large compressive deformations, as well as efficient fire-resistance. The bending capability and increased contacts of crosslinked graphene-based cell walls upon a compressive deformation significantly improve strain/pressure sensing sensitivity with respect to the neat RGO aerogels, showing the advantages of cost-effective macromolecule-derived carbons for improving the sensing performance in the graphene-based aerogels. The ultralight aerogel sensors can be operated at an ultralow voltage of 0.2 V and a low power consumption that is below 2.0 mW. They can also be successfully used to detect a wide range of strains, from 0.1% to 80.0%, in a wide temperature range, from room temperature to more than 300 °C. The crosslinked graphene aerogel sensors also achieve an ultrahigh pressure sensitivity of 10 kPa^{-1} in a wide pressure range, from 13 to 2750 Pa, and excellent sensing stability and durability. Moreover, the aerogel sensors sense the vibration signals with ultrahigh frequencies of up to 4000 Hz at more than 1, 000, 000 cycles, significantly outperforming those of other sensors. The high flexibility and robustness, ultralow density, and excellent piezoresistive sensing capability of the crosslinked graphene biomimetic aerogel sensors make them promising wearable sensors for

sensitive and reliable monitoring of various mechanical signals and human motions with various frequencies or amplitudes, and non-destructive monitoring of cracks on engineering structures.

Experimental

Preparation of macromolecule-derived carbon crosslinked graphene-based biomimetic aerogel sensors. 0.6 wt% GO aqueous dispersion (prepared by a modified Hummer's method as shown in our previous work [28]) and 0.6 wt% of a macromolecule such as lignin (USA, TCI product number: L0082, soft lignin) or PVA (USA, Average Mw 85000-124000, 87-89 % hydrolyzed, Aldrich Chemistry) aqueous dispersion were mixed in the desired ratio using a magnetic stirring bar for two hours. The GO/PDA mixed dispersion was prepared by adding dopamine hydrochloride (DA, 98%, Aldrich Chemistry) into 0.6 wt% GO dispersion that had already been mixed with 0.4 wt% tris(hydroxymethyl)aminomethane (Tris, 99%, Aldrich Chemistry) by magnetic stirring for 4 h, followed by stirring the dispersion for 24 h and adjusting the water to achieve the desired concentration.[38] The GO/macromolecule mixed dispersion was subsequently poured into a Teflon mold with stainless steel as cold finger immersed in the liquid nitrogen for freezing process. A steep temperature gradient provided by liquid nitrogen resulted in a unidirectional ice crystal growth that started from the cold finger in the mixed dispersion. Following the roughly 24 h freeze-drying process in a freeze-drying vessel (–80 ºC and 10 Pa), the microhoneycomb GO/macromolecule composite aerogels with aligned cell walls were obtained. The attained GO/macromolecule aerogels were heated at a rate of 5 ºC/min in a tube furnace and annealed at the temperature of 800 ºC for 2 h in an argon atmosphere, resulting in the successful fabrication of the carbon crosslinked graphene based microhoneycomb aerogels. Using the thermogravimetric analysis of these precursors, the

corresponding mass ratios of macromolecule-derived carbon in the hybrid aerogels were also calculated. Herein, neat PVAC and PDAC aerogels would collapse because of their low mechanical strength at ultralow densities while LDC aerogels could have a stable structure. Therefore, the LDC was selected as the representative macromolecule-derived carbon to describe its influence on the properties of the crosslinked graphene-based biomimetic aerogels.

Characterization. The microstructure was investigated with scanning electron microscopy (SEM, JSM-7600F). X-ray diffraction (XRD) curves were obtained by a specular reflection mode (Cu Ka radiation, PANalytical, Holland) at room temperature. Raman spectra were obtained with a Renishaw Raman Spectroscope using the 632.8 nm line of a He-Ne laser. The compression behavior of the aerogels was evaluated with a dynamic mechanical analyzer (DMA, TA Q800), and for each component of aerogel at least five samples were tested. Unless specifically mentioned, the compressive direction was perpendicular to the honeycomb pore channels of the aerogels. An autolab apparatus (Metrohm Autolab, the Netherlands) was used to measure the electrical properties with a two-probe setup on the sensors and an applied voltage was 0.2 V. In order to achieve good electric contact, a silver paste was coated on two opposite sides of the samples. In the sensing test for high-frequency mechanical vibration, the electric signals were recorded by an oscilloscope (Agilent® DSO9064A).

Supporting Information

Supporting Information is available from the Wiley Online Library or from the author.

Acknowledgements
Z Zeng and N Wu contributed equally to this work. This work was supported by Science and Engineering Research Council of the Agency for Science, Technology and Research (A*STAR) Singapore under Public Sector Research Funding (PSF) Grant No. 1521200077, and the Qilu Young Scholar Program of Shandong University (No. 31370082163127).

Received: ((will be filled in by the editorial staff))
Revised: ((will be filled in by the editorial staff))
Published online: ((will be filled in by the editorial staff))

REFERENCES

[1] a) C. S. Boland, U. Khan, G. Ryan, S. Barwich, R. Charifou, A. Harvey, C. Backes, Z. Li, M. S. Ferreira, M. E. Möbius, R. J. Young, J. N. Coleman, *Science* **2016**, *354*, 1257; b) G. Schwartz, B. C. Tee, J. Mei, A. L. Appleton, D. H. Kim, H. Wang, Z. Bao, *Nat. Commun.* **2013**, *4*, 1859; c) Z.-L. Yu, B. Qin, Z.-Y. Ma, J. Huang, S.-C. Li, H.-Y. Zhao, H. Li, Y.-B. Zhu, H.-A. Wu, S.-H. Yu, *Adv. Mater.* **2019**, *31*, 1900651; d) C. Li, Y.-W. Ding, B.-C. Hu, Z.-Y. Wu, H.-L. Gao, H.-W. Liang, J.-F. Chen, S.-H. Yu, *Adv. Mater.* **2020**, *32*, 1904331; e) Y. Si, J. Yu, X. Tang, J. Ge, B. Ding, *Nat. Commun.* **2014**, *5*, 5802.

[2] Z. Chen, W. Ren, L. Gao, B. Liu, S. Pei, H.-M. Cheng, *Nat. Mater.* **2011**, *10*, 424.

[3] H. Zhuo, Y. Hu, Z. Chen, X. Peng, L. Liu, Q. Luo, J. Yi, C. Liu, L. Zhong, *J. Mater. Chem. A* **2019**, *7*, 8092.

[4] X. Li, T. Yang, Y. Yang, J. Zhu, L. Li, F. E. Alam, X. Li, K. Wang, H. Cheng, C.-T. Lin, Y. Fang, H. Zhu, *Adv. Funct. Mater*. **2016**, *26*, 1322.

[5] Y. Cheng, R. Wang, J. Sun, L. Gao, *Adv. Mater.* **2015**, *27*, 7365.

[6] Z. Y. Wu, C. Li, H. W. Liang, J. F. Chen, S. H. Yu, *Angew. Chem. Int. Ed*. **2013**, *52*, 2925.

[7] Y. Si, X. Wang, C. Yan, L. Yang, J. Yu, B. Ding, *Adv. Mater.* **2016**, *28*, 9512.

[8] a) A. D. Smith, F. Niklaus, A. Paussa, S. Vaziri, A. C. Fischer, M. Sterner, F. Forsberg, A. Delin, D. Esseni, P. Palestri, M. Ostling, M. C. Lemme, *Nano Lett.* **2013**, *13*, 3237; b) S. Chen, K. Jiang, Z. Lou, D. Chen, G. Shen, *Adv. Mater. Technol.* **2018**, *3*, 1700248; c) Z. Lou, S. Chen, L. Wang, K. Jiang, G. Shen, *Nano Energy* **2016**, *23*, 7; d) Q. Liu, J. Chen, Y. Li, G. Shi, *ACS Nano* **2016**, *10*, 7901.

[9] C. Wu, X. Huang, X. Wu, R. Qian, P. Jiang, *Adv. Mater.* **2013**, *25*, 5658.

[10] a) K. Pang, X. Song, Z. Xu, X. Liu, Y. Liu, L. Zhong, Y. Peng, J. Wang, J. Zhou, F. Meng, J. Wang, C. Gao, *Sci. Adv.* **2020**, *6*, eabd4045; b) H. Kashani, Y. Ito, J. Han, P. Liu, M. Chen, *Sci. Adv.* **2019**, *5*, eaat6951.

[11] H. L. Gao, Z. Y. Wang, C. Cui, J. Z. Bao, Y. B. Zhu, J. Xia, S. M. Wen, H. A. Wu, S. H. Yu, *Adv. Mater.* **2021**, *33*, e2102724.

[12] R. Zhang, R. Hu, X. Li, Z. Zhen, Z. Xu, N. Li, L. He, H. Zhu, *Adv. Funct. Mater.* **2018**, *28*, 1705879.

[13] T. Yang, W. Wang, H. Zhang, X. Li, J. Shi, Y. He, Q.-s. Zheng, Z. Li, H. Zhu, *ACS Nano* **2015**, *9*, 10867.

[14] J. Kuang, L. Liu, Y. Gao, D. Zhou, Z. Chen, B. Han, Z. Zhang, *Nanoscale* **2013**, *5*, 12171.

[15] L. Qiu, J. Z. Liu, S. L. Chang, Y. Wu, D. Li, *Nat. Commun.* **2012**, *3*, 1241.

[16] H. Zhuo, Y. Hu, X. Tong, Z. Chen, L. Zhong, H. Lai, L. Liu, S. Jing, Q. Liu, C. Liu, X. Peng, R. Sun, *Adv. Mater.* **2018**, *30*, e1706705.

[17] K. Zhao, T. Zhang, H. Chang, Y. Yang, P. Xiao, H. Zhang, C. Li, C. S. Tiwary, P. M. Ajayan, Y. Chen, *Sci. Adv.* **2019**, *5*, eaav2589.

[18] L. Qiu, B. Huang, Z. He, Y. Wang, Z. Tian, J. Z. Liu, K. Wang, J. Song, T. R. Gengenbach, D. Li, *Adv. Mater.* **2017**, *29*, 1701553.

[19] H.-L. Gao, Y.-B. Zhu, L.-B. Mao, F.-C. Wang, X.-S. Luo, Y.-Y. Liu, Y. Lu, Z. Pan, J. Ge, W. Shen, Y.-R. Zheng, L. Xu, L.-J. Wang, W.-H. Xu, H.-A. Wu, S.-H. Yu, *Nat. Commun.* **2016**, *7*, 12920.

[20] L. Qiu, M. Bulut Coskun, Y. Tang, J. Z. Liu, T. Alan, J. Ding, V. T. Truong, D. Li, *Adv. Mater.* **2016**, *28*, 194.

[21] C. S. Boland, U. Khan, C. Backes, A. O'Neill, J. McCauley, S. Duane, R. Shanker, Y. Liu, I. Jurewicz, A. B. Dalton, J. N. Coleman, *ACS Nano* **2014**, *8*, 8819.

[22] H. Xu, Z. Zeng, Z. Wu, L. Zhou, Z. Su, Y. Liao, M. Liu, *Compos. Sci. Technol.* **2017**, *149*, 246.

[23] a) Z. Ma, A. Wei, J. Ma, L. Shao, H. Jiang, D. Dong, Z. Ji, Q. Wang, S. Kang, *Nanoscale* **2018**, *10*, 7116; b) P. Lv, K. Yu, X. Tan, R. Zheng, Y. Ni, Z. Wang, C. Liu, W. Wei, *RSC Adv.* **2016**, *6*, 11256; c) P. Lv, X.-W. Tan, K.-H. Yu, R.-L. Zheng, J.-J. Zheng, W. Wei, *Carbon* **2016**, *99*, 222.

[24] J. Kuang, Z. Dai, L. Liu, Z. Yang, M. Jin, Z. Zhang, *Nanoscale* **2015**, *7*, 9252.

[25] Y. Qin, Q. Peng, Y. Ding, Z. Lin, C. Wang, Y. Li, F. Xu, J. Li, Y. Yuan, X. He, Y. Li, A*CS Nano* **2015**, *9*, 8933.

[26] a) H. Liu, M. Dong, W. Huang, J. Gao, K. Dai, J. Guo, G. Zheng, C. Liu, C. Shen, Z. Guo, *J. Mater. Chem. C* **2017**, *5*, 73; b) B.-X. Zhang, Z.-L. Hou, W. Yan, Q.-L. Zhao, K.-T. Zhan, *Carbon* **2017**, *125*, 199.

[27] H. B. Yao, J. Ge, C. F. Wang, X. Wang, W. Hu, Z. J. Zheng, Y. Ni, S. H. Yu, *Adv. Mater.* **2013**, *25*, 6692.

[28] Z. Zeng, S. I. Seyed Shahabadi, B. Che, Y. Zhang, C. Zhao, X. Lu, *Nanoscale* **2017**, *9*, 17396.

[29] S.-X. Wang, L. Yang, L. P. Stubbs, X. Li, C. He, *ACS Appl. Mater. Interfaces* **2013**, *5*, 12275.

[30] T. Ma, H. L. Gao, H. P. Cong, H. B. Yao, L. Wu, Z. Y. Yu, S. M. Chen, S. H. Yu, *Adv. Mater.* **2018**, *30*, e1706435.

[31] Z. Zeng, E. Mavrona, D. Sacre, N. Kummer, J. Cao, L. A. E. Muller, E. Hack, P. Zolliker, G. Nystrom, *ACS Nano* **2021**, *15*, 7451.

[32] Z. Zeng, C. Wang, G. Siqueira, D. Han, A. Huch, S. Abdolhosseinzadeh, J. Heier, F. Nuesch, C. J. Zhang, G. Nystrom, *Adv. Sci.* (Weinh) **2020**, *7*, 2000979.

[33] Z. Zeng, T. Wu, D. Han, Q. Ren, G. Siqueira, G. Nystrom, *ACS Nano* **2020**, *14*, 2927.

[34] Z. Zeng, C. Wang, T. Wu, D. Han, M. Luković, F. Pan, G. Siqueira, G. Nyström, *J. Mater. Chem. A* **2020**, *8*, 17969.

[35] Y.-J. Wan, P.-L. Zhu, S.-H. Yu, R. Sun, C.-P. Wong, W.-H. Liao, *Carbon* **2017**, *115*, 629.

[36] Y. Li, B. Shen, X. Pei, Y. Zhang, D. Yi, W. Zhai, L. Zhang, X. Wei, W. Zheng, *Carbon* **2016**, *100*, 375.

[37] L. Pan, A. Chortos, G. Yu, Y. Wang, S. Isaacson, R. Allen, Y. Shi, R. Dauskardt, Z. Bao, *Nat. Commun*. **2014**, *5*, 3002.

[38] Y. Hu, Z. Chen, H. Zhuo, L. Zhong, X. Peng, R. C. Sun, *Adv. Funct. Mater.* **2019**, *29,* 1904472.

[39] D. Kang, P. V. Pikhitsa, Y. W. Choi, C. Lee, S. S. Shin, L. Piao, B. Park, K. Y. Suh, T. I. Kim, M. Choi, *Nature* **2014**, *516*, 222.

[40] D. J. Lipomi, M. Vosgueritchian, B. C. Tee, S. L. Hellstrom, J. A. Lee, C. H. Fox, Z. Bao, *Nat. Nanotechnol.* **2011**, *6*, 788.

[41] X. Xiao, L. Yuan, J. Zhong, T. Ding, Y. Liu, Z. Cai, Y. Rong, H. Han, J. Zhou, Z. L. Wang, *Adv. Mater.* **2011**, *23*, 5440.

[42] M. Amjadi, M. Turan, C. P. Clementson, M. Sitti, *ACS Appl. Mater. Interfaces* **2016**, *8*, 5618.

[43] S. Gong, D. T. Lai, Y. Wang, L. W. Yap, K. J. Si, Q. Shi, N. N. Jason, T. Sridhar, H. Uddin, W. Cheng, *ACS Appl. Mater. Interfaces* **2015**, *7*, 19700.

[44] T. N. Tallman, S. Gungor, K. W. Wang, C. E. Bakis, *Carbon* **2015**, *95*, 485.

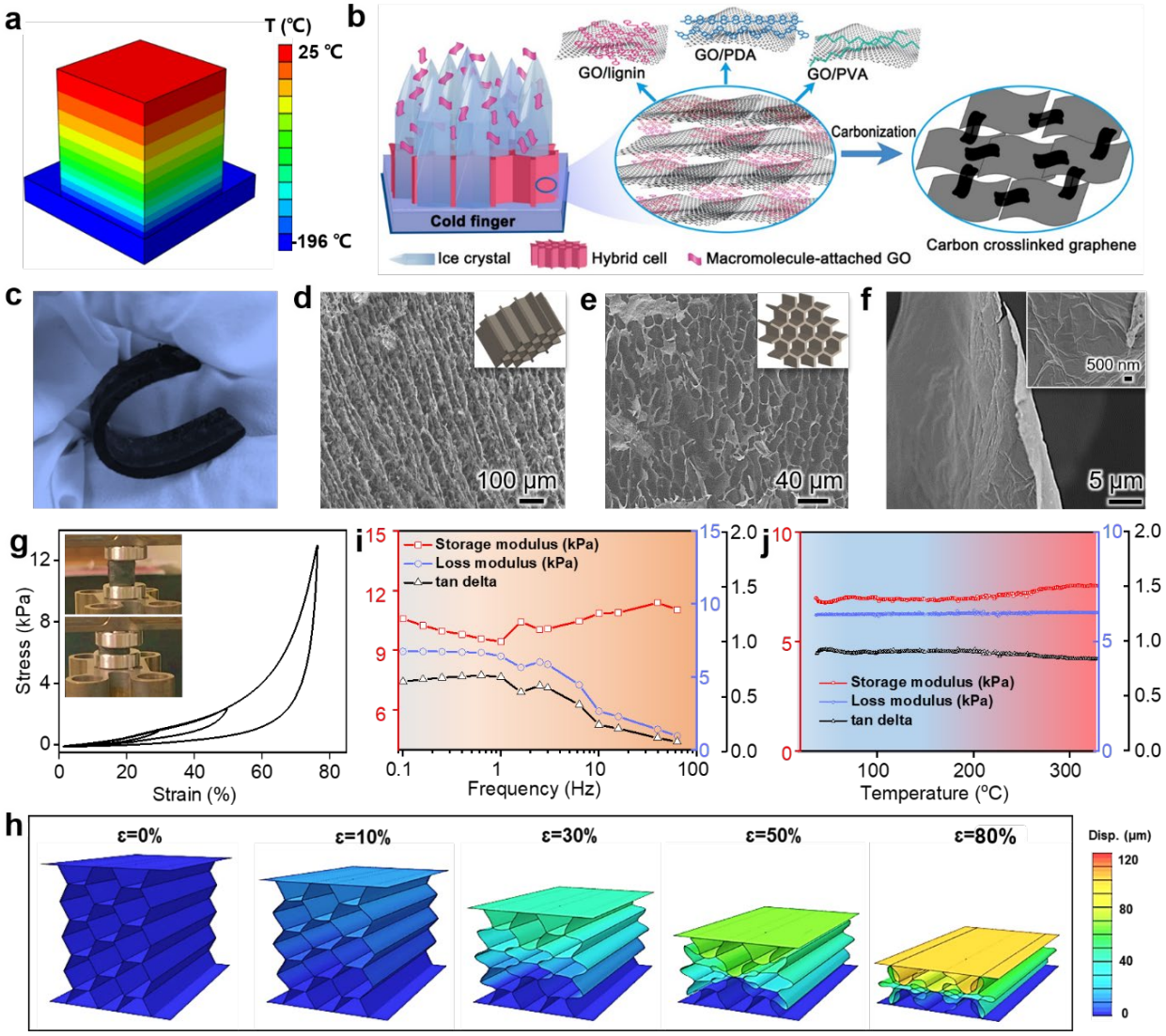

Figure 1. Preparation, structure, and mechanical performance. (a) A FE simulation showing the temperature gradient in the unidirectional freezing process. (b) A schematic showing the preparation of the sustainable macromolecules assisted crosslinked graphene-based aerogels sensors. (c) A typical optical image of the ultralight (~3.5 mg/cm^3), crosslinked graphene aerogel sensor bent in one's hand showing the great mechanical robustness and flexibility. SEM images in the (d) longitudinal and (e) transverse planes of the aerogel, (f) SEM image of the crosslinked graphene-based cell walls (inset shows the intercalation of carbon between graphene layers and the crosslink of graphene layers in the cell walls). (g) Typical stress-strain curve of the crosslinked graphene aerogel sensor during cyclic compressions with various strains. (h) The simulated model with similar microhoneycomb porous structure of the crosslinked graphene aerogel sensor showing the true material deformation under various compression strains. The (i) frequency and (j) temperature dependence of storage modulus, loss modulus, and damping ratio of the crosslinked graphene aerogel sensor.

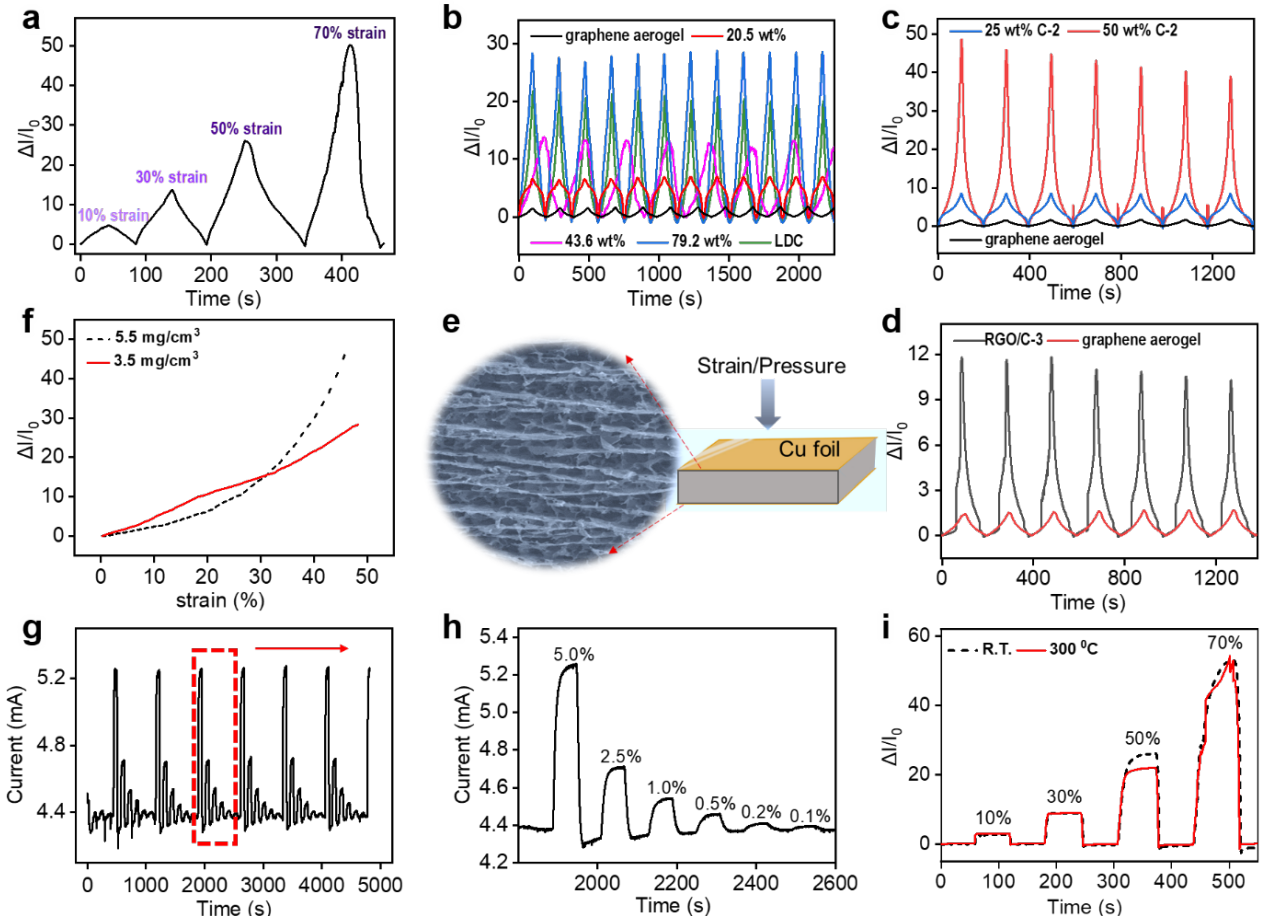

Figure 2. Strain sensing performance of the ultralight, crosslinked graphene-based aerogel sensors. (a) $\Delta I/I_0$ value of the aerogel sensors at various large compressive strains, (b) the $\Delta I/I_0$ of the aerogel sensors with various LDC mass ratios at a cyclic 50 % compressive strain. $\Delta I/I_0$ of the (c) PDAC (C-2) crosslinked graphene aerogel sensors prepared from GO/PDA composite aerogels with different carbon contents (d) 50 wt% PVAC (C-3) crosslinked graphene aerogels when the samples are subjected to a cyclic compressive strain of 50 %. (e) The schematic showing the compression strain sensing experiment and process. (f) The crosslinked graphene-based aerogel sensors with different densities as a function of compressive strain. (g, h) The current change of the aerogel sensors at various small deformations. (i) The $\Delta I/I_0$ of the aerogel sensor upon various compressive ratios at temperatures of 25 and 300 °C.

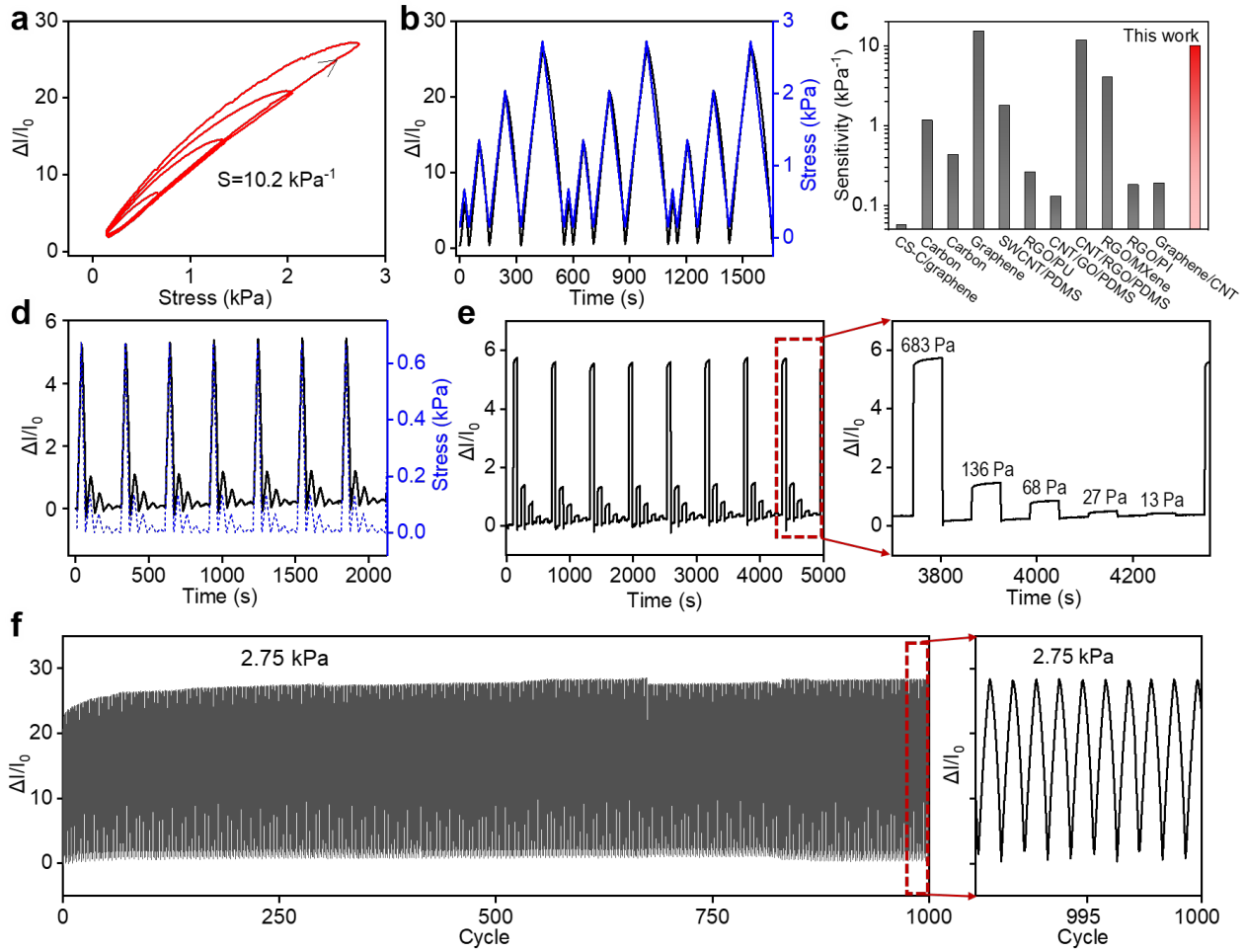

Figure 3. Pressure sensing performance of the ultralight, crosslinked graphene-based aerogel sensors. (a) The $\Delta I/I_0$ of the aerogel sensors at a cyclic compressive stress and the sensing sensitivity (*S*), (b) the cyclic $\Delta I/I_0$ of the aerogel sensors at various large compressive stresses, (c) the comparison in sensing sensitivity of typical carbon-based pressure sensors (the experimental data and source reference used in this figure are shown in Table S1). (d, e) The $\Delta I/I_0$ of the aerogel sensors at various small compressive stresses. (f) Long life-time of the aerogel pressure sensors.

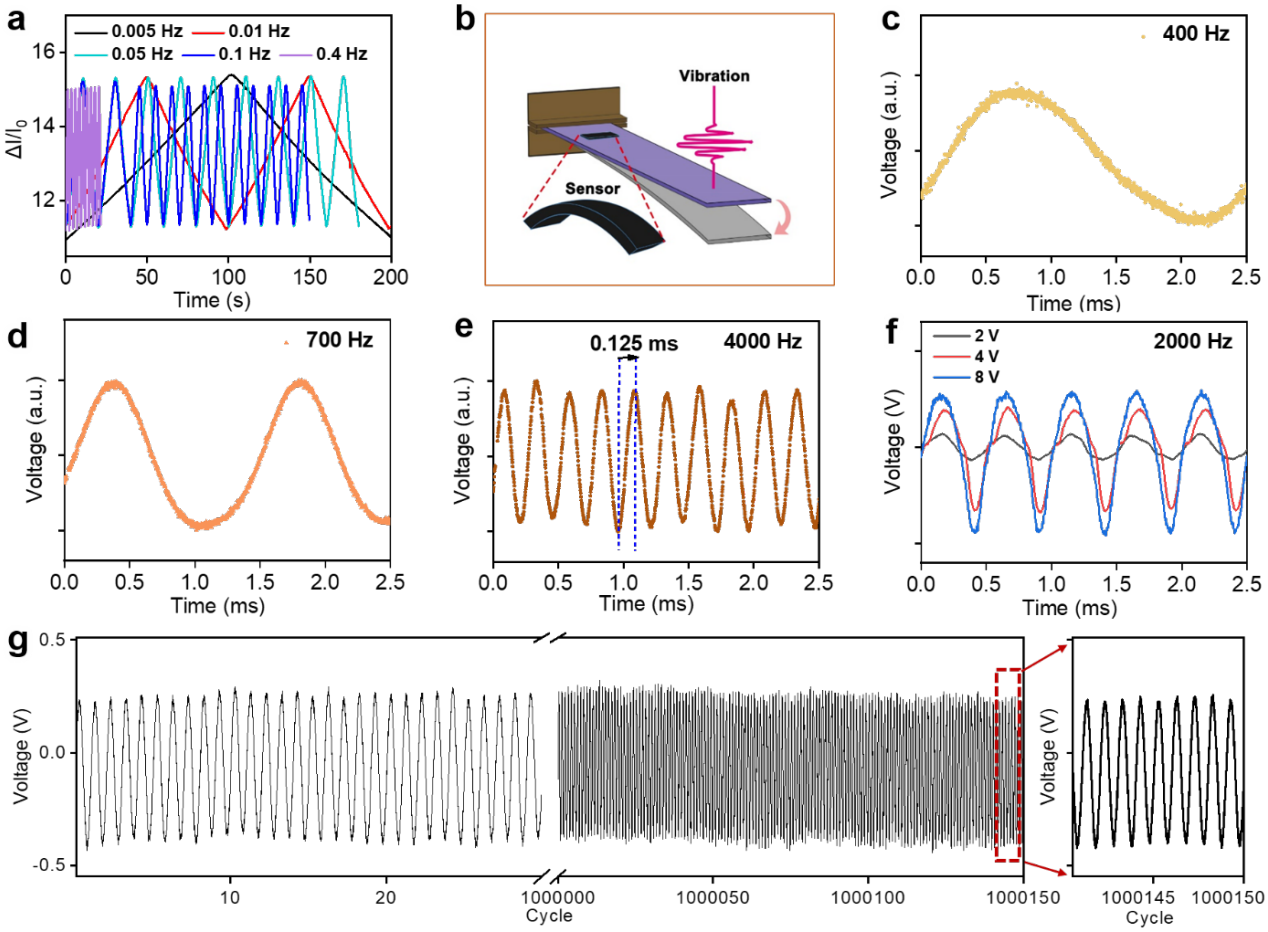

Figure 4. Low-frequency strain/pressure to high-frequency vibration sensing performance of the ultralight, crosslinked graphene-based aerogel sensors. (a) The response electric signals to various pressure frequencies for the aerogel sensors. (b) Schematic of the sensing test of the high-frequency vibration signals for the aerogel sensor. The mechanical shaker (B&K® 4809) leads to the vibration of the solid board with controlled frequency, which leads to the vibration of the sensors with subtle yet high-frequency mechanical deformations. Response of the aerogel sensor to a (c) 400 Hz, (d) 700 Hz, and (e) 4000 Hz vibration signals, and (f) response of the aerogel sensor to 2000 Hz vibrations with various amplitudes caused by the shaker. (g) Extremely long cyclic tests with a vibration signal of more than 1 million cycles, showing the excellent durability and reliability of the aerogel-based vibration sensors.

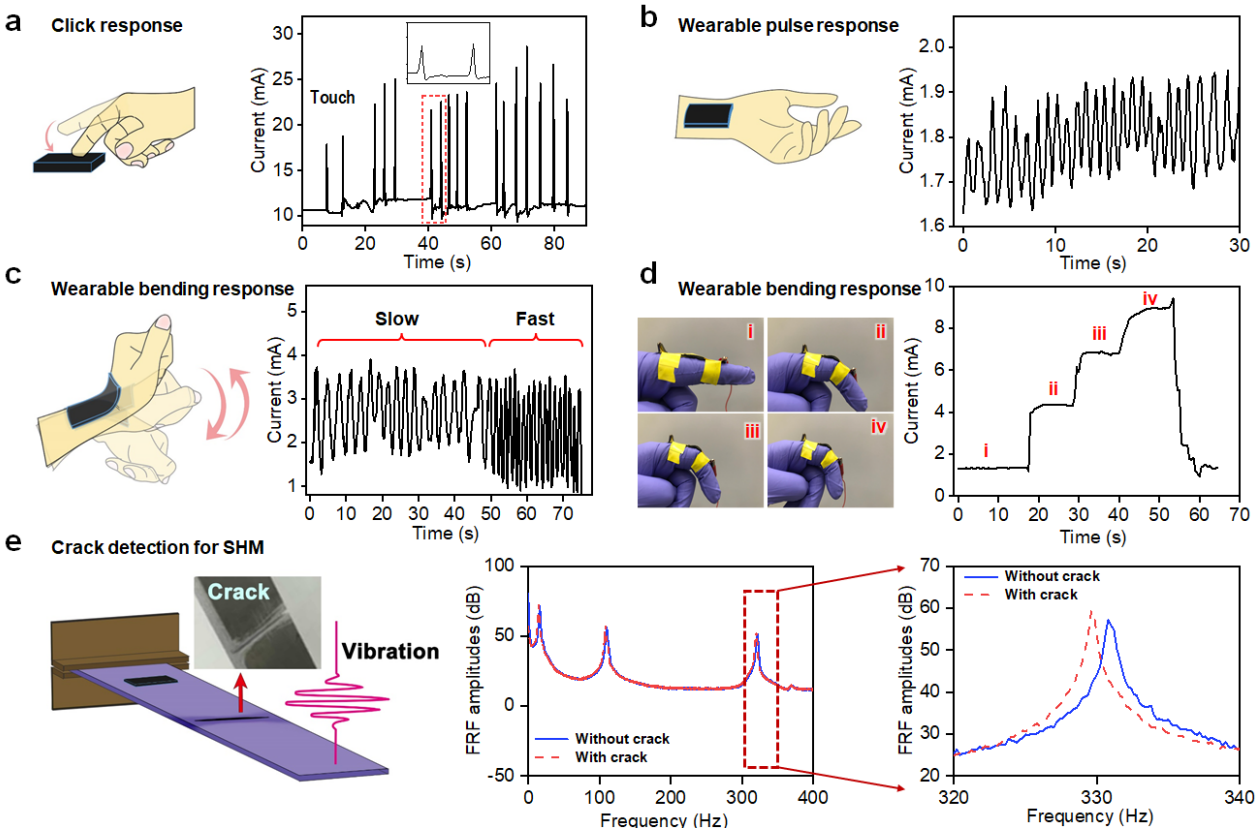

Figure 5. Application demonstration of the ultralight, crosslinked graphene-based aerogel sensors. (a) The response current to the finger touch of the aerogel sensors. Detecting the (b) pulse, (c) bent wrist, and (d) bent fingers of the wearable aerogel sensors. (e) Aerogel based vibration sensors for structural health monitoring application, showing the efficient detection of a crack on the engineering structure (cantilever beam).

Table 1. Frequency sensitivity of typical sensors ever reported

Material	Response frequency	Sensing signla	Reference
Crosslinked graphene aerogel sensor	**0.005 - 4000 Hz**	**Cycle compression & Vibration**	**This work**
Platinum (Pt)-PDMS	200 Hz vibration; ＜ 2 kHz sound wave	Crack-based sensor	[39] Nature 2014
Graphene foam	2 kHz	Vibration	[20] Adv Mater 2016
Aligned CNT-PDMS	/	Breathing response	[40]Nat Nanotechnol 2011
ZnO nanowire/PDMS	2 Hz		[41]Adv Mater 2011
Graphene-rubber composite	160 Hz	Vibration	[21]ACS Nano 2014
Graphene /PEI foam	0.167 Hz	Cycle compression	[25]ACS Nano 2015
Graphene woven microfabrics	100 Hz	Acoustic vibration	[13]ACS Nano 2015
Microcracked graphite - elastomer	99 Hz	Sound wave	[42]ACS AMI 2016
AuNW/PANI-rubber	1 Hz		[43]ACS AMI 2015
Hierarchical graphene foam	0.4 Hz	Cycle compression	[14]Nanoscale 2013
CNF/PU nanocomposite	0.0125 Hz	Cycle tension	[44]Carbon 2015

Supporting Information

Sustainable Macromolecules Assisted Preparation of Cross-linked, Ultralight, Flexible Graphene Aerogel Sensors toward Low-Frequency Strain/Pressure to High-Frequency Vibration Sensing

Prof. Z. Zeng

Key Laboratory for Liquid-Solid Structural Evolution and Processing of Materials, Ministry of Education and School of Materials Science and Engineering, Shandong University, Jinan, Shandong, 250061, China

*E-mail: zhihui.zeng@sdu.edu.cn (Z. Zeng),

Prof. Z. Zeng, Prof. X. Lu,

School of Materials Science and Engineering, Nanyang Technological University, 50 Nanyang Avenue, Singapore 639798, Singapore

*E-mail:asxhlu@ntu.edu.sg (X. Lu);

Dr. N. Wu

Department of Chemistry and Applied Biosciences, ETH Zurich, CH-8093 Zurich, Switzerland

Prof. W. Yang

School of Aerospace Engineering and Applied Mechanics, Tongji University, Shanghai 200092, China

Assoc. Prof. H. Xu

School of Aeronautics and Astronautics, Dalian University of Technology, Dalian, China

Dr. Y. Liao, Prof. Z. Su

Department of Mechanical Engineering, The Hong Kong Polytechnic University, Kowloon, Hong Kong

Dr. M. Luković

Swiss Federal Laboratories for Materials Science and Technology (EMPA), Überlandstrasse 129, 8600 Dübendorf, Switzerland

Video S1. One hybrid aerogel with good fire-resistance.

Video S2. The press to the aerogel sensors and corresponding current signals.

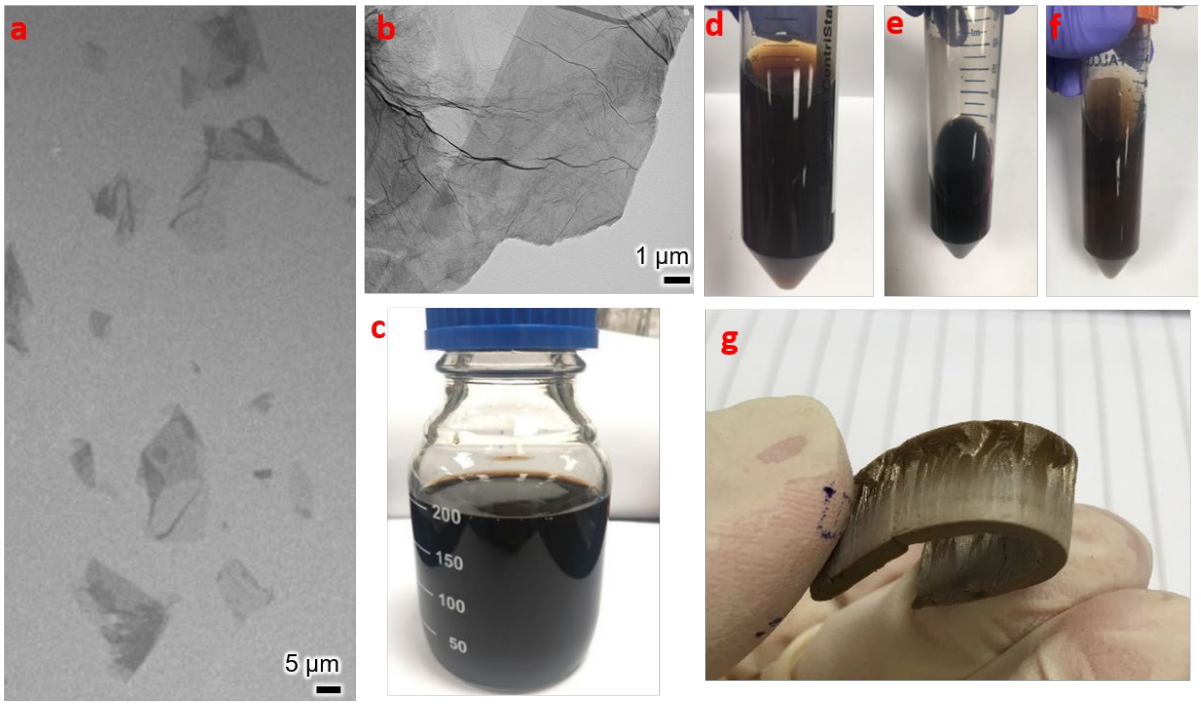

Figure S1. (a) SEM and (b) TEM images of the as-prepared GO layers. Images of the (c) GO, (d) GO/lignin, (e) GO/PDA, and (f) GO/PVA mixed dispersion, (g) flexible lignin crosslinked microhoneycomb GO aerogels, (d) TGA curves of the GO/lignin aerogels with different GO/lignin ratios. A thermogravimetric analyzer (TGA, TA Instrument Q500) was employed to study the mass change.

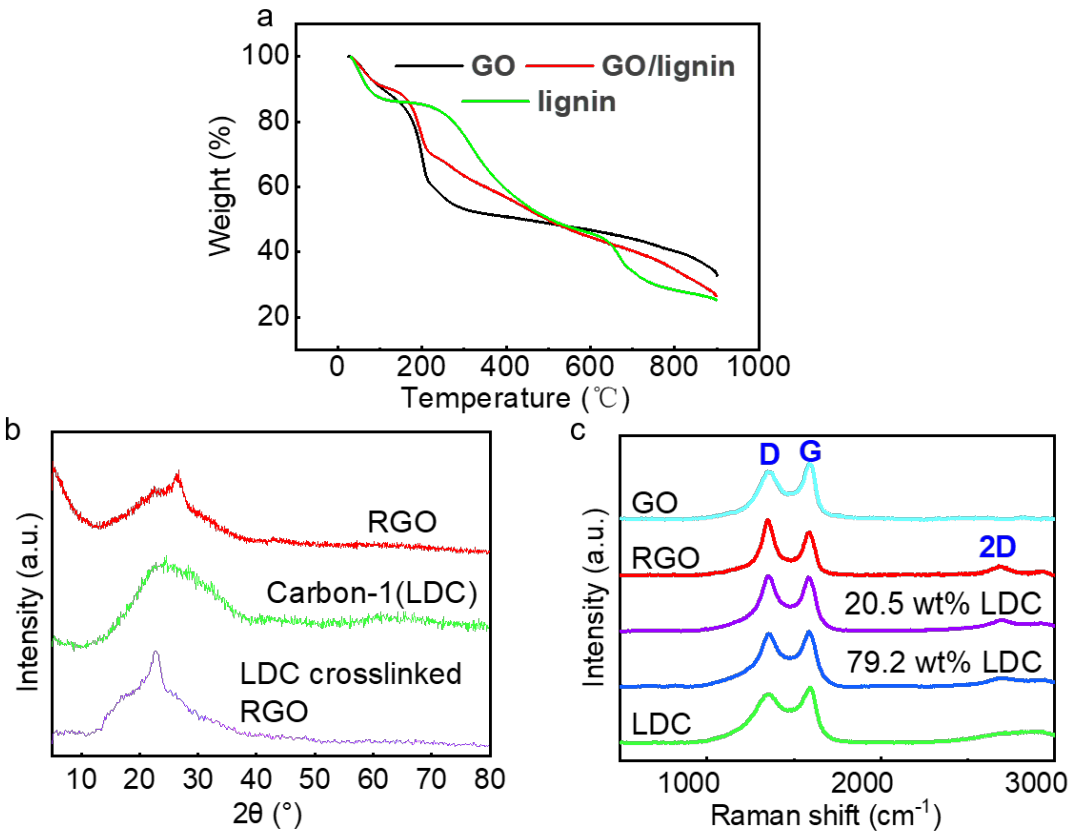

Figure S2. (a) TGA curves of the GO/lignin aerogels with different GO/lignin ratios, showing the mass change during the annealing process. A thermogravimetric analyzer (TGA, TA Instrument Q500) was employed to study the mass change. (b) XRD patterns and (c) Raman spectra of the as-prepared carbon-based aerogels

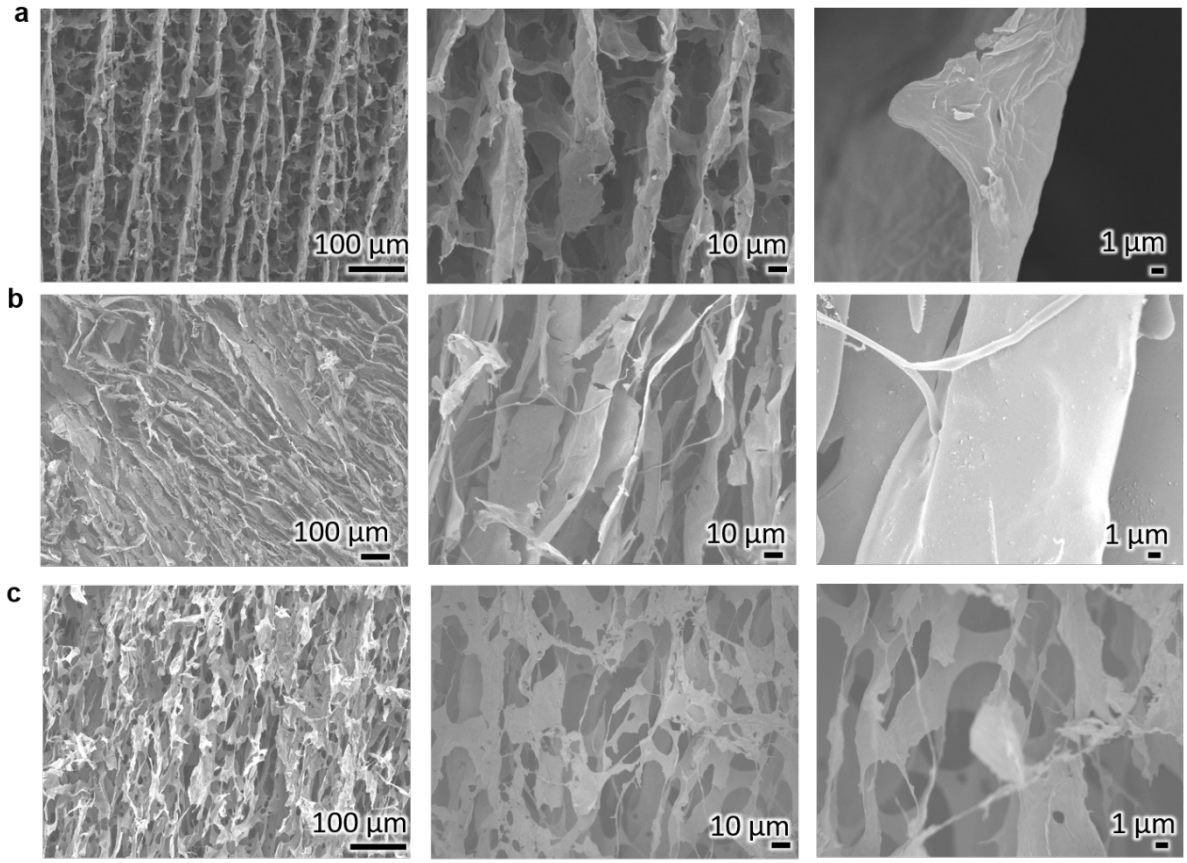

Figure S3. Microstructure of the (a) LDC crosslinked graphene-based aerogel sensors, (c) LDC aerogels, and (d) graphene aerogels without crosslink.

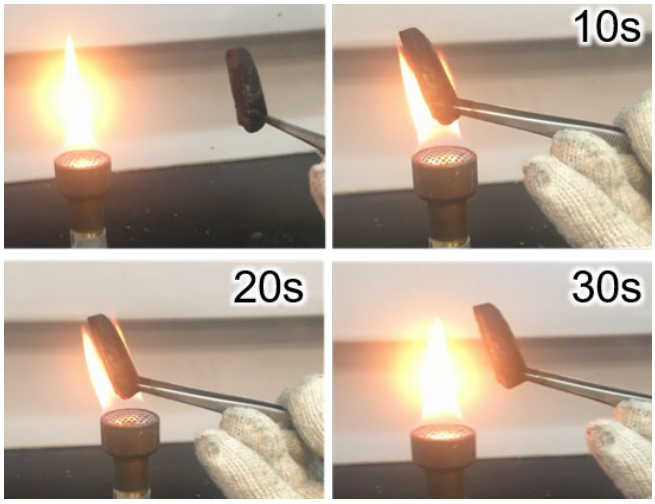

Figure S4. The fire-resistance of the crosslinked graphene aerogel sensors.

Figure S5. Optical images showing the reversible compressions of the crosslinked graphene-based aerogels with a strain of 80%.

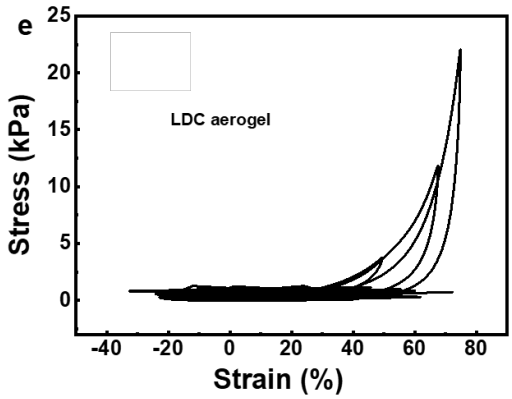

Figure S6. Irreversible compression of pure LDC aerogels at a strain beyond 70%.

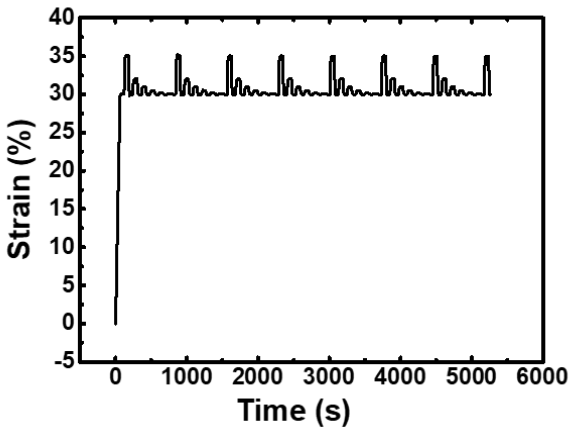

Figure S7. Strains change of the sensors for the test of small deformations.

Table S1. Comparison of sensistivity of the crosslinked graphene baed sensors with previously reported carbon based pressure sensors.

Sensor	Sensitivity (kPa^{-1})	Density (mg/cm^3)	Reference
Crosslinked graphene micro honeycomb aerogel	**10.2**	**3.5**	**This work**
Carbon/graphene lamellar	1.17	11	[1] Adv Mater 2021
Carbon	0.057		[2] Adv Mater 2019
Carbon	0.43		[3] Adv Mater 2016
Graphene	15.2		[4] Adv Mater 2014
SWCNTs@PDMS	1.8		[5] Adv Mater 2014
RGO@PU	0.26		[6] Adv Mater 2013
CNTs/GO@PDMS	0.13		[7] Adv Funct Mater 2018
CNTS/RGO-CNF	11.82		[8] J Mater Chem A 2018
RGO/MXene	4.05		[9] ACS Nano 2018
RGO@PI	0.18		[10] ACS Nano 2015
Graphene/CNTs	0.19		[11] Nanoscale 2015

[1] H. L. Gao, Z. Y. Wang, C. Cui, J. Z. Bao, Y. B. Zhu, J. Xia, S. M. Wen, H. A. Wu, S. H. Yu, Adv. Mater. **2021**, 33, e2102724.

[2] Z. L. Yu, B. Qin, Z. Y. Ma, J. Huang, S. C. Li, H. Y. Zhao, H. Li, Y. B. Zhu, H. A. Wu, S. H. Yu, Adv. Mater. **2019**, 31, 1900651.

[3] Y. Si, X. Wang, C. Yan, L. Yang, J. Yu, B. Ding, Adv. Mater. **2016**, 28, 9512.

[4] C. Y. Hou, H. Z. Wang, Q. H. Zhang, Y. G. Li, M. F. Zhu, Adv. Mater. **2014**, 26, 5018.

[5] X. W. Wang, Y. Gu, Z. P. Xiong, Z. Cui, T. Zhang, Adv. Mater. **2014**, 26, 1336.

[6] H. B. Yao, J. Ge, C. F. Wang, X. Wang, W. Hu, Z. J. Zheng, Y. Ni, S. H. Yu, Adv. Mater. **2013**, 25, 6692.

[7] C. H. Mu, Y. Q. Song, W. T. Huang, A. Ran, R. J. Sun, W. H. Xie, H. W. Zhang, Adv. Funct. Mater. **2018**, 28, 1707503.

[8] X. Peng, K. Wu, Y. Hu, H. Zhuo, Z. Chen, S. Jing, Q. Liu, C. Liu, L. Zhong, J. Mater. Chem. A **2018**, 6, 23550.

[9] Y. N. Ma, Y. Yue, H. Zhang, F. Cheng, W. Q. Zhao, J. Y. Rao, S. J. Luo, J. Wang, X. L. Jiang, Z. T. Liu, N. S. Liu, Y. H. Gao, ACS Nano **2018**, 12, 3209.

[10] Y. Y. Qin, Q. Y. Peng, Y. J. Ding, Z. S. Lin, C. H. Wang, Y. Li, J. J. Li, Y. Yuan, X. D. He, Y. B. Li, ACS Nano **2015**, 9, 8933.

[11] J. Kuang, Z. H. Dai, L. Q. Liu, Z. Yang, M. Jin, Z. Zhang, Nanoscale **2015**, 7, 9252.